Available online at www.sciencedirect.com
ScienceDirect
Geochimica et Cosmochimica Acta 73 (2009) 5361–5376
Geochimica et Cosmochimica Acta
www.elsevier.com/locate/gca

Inorganic synthesis of Fe–Ca–Mg carbonates at low temperature

Christopher S. Romanek [a,b,*], Concepción Jiménez-López [c,*], Alejandro Rodriguez Navarro [d], Monica Sánchez-Román [a,b], Nita Sahai [e], Max Coleman [f]

[a] NASA Astrobiology Institute and Department of Geology, University of Georgia, Athens, GA 30602, USA
[b] Savannah River Ecology Laboratory, Aiken, SC 29802, USA
[c] Departamento de Microbiologia, Facultad de Ciencias, Universidad de Granada, Granada, Spain
[d] Departamento de Mineralogía y Petrología, Facultad de Ciencias, Universidad de Granada, Granada, Spain
[e] NASA Astrobiology Institute and Department of Geology and Geophysics, University of Wisconsin-Madison, 1215 W. Dayton St., Madison, WI 53706, USA
[f] NASA Astrobiology Institute and Jet Propulsion Laboratory, California Institute of Technology, M/S 183-301, 4800 Oak Grove Drive, Pasadena, CA 91109, USA

Received 14 January 2009; accepted in revised form 26 May 2009; available online 11 June 2009

Abstract

A set of free-drift experiments was undertaken to synthesize carbonates of mixed cation content (Fe, Ca, Mg) from solution at 25 and 70 °C to better understand the relationship between the mineralogy and composition of these phases and the solutions from which they precipitate. Metastable solid solutions formed at 25 °C which are not predicted from the extrapolation of higher temperature equilibrium assemblages; instead, solids formed that were intermediary in chemical composition to known magnesite–siderite and dolomite solid solutions. A calcite–siderite solid solution precipitated at 25 °C, with the percentage of $CaCO_3$ in the solid being proportional to the aqueous Ca/Fe ratio of the solution, while Mg was excluded from the crystal structure except at relatively high aqueous Mg/Ca and Mg/Fe ratios and a low Ca content. Alternatively, at 70 °C Mg was the predominant cation of the solid solutions. These results are compatible with the hypothesis that the relative dehydration energies of Fe, Ca and Mg play an important role in the formation of mixed cation carbonates in nature.

1. INTRODUCTION

1.1. The formation of siderite

Siderite is a crystalline carbonate containing >50 mol% $FeCO_3$. It is found in sediments and rocks of all ages (James, 1966; Garrels et al., 1973; Hangari et al., 1980; Maynard, 1982; Thyne and Gwinn, 1994; Fisher et al., 1998) and it forms in a broad range of terrestrial environments (e.g., Bricker, 1975; Emerson, 1976; Matsumoto and Iijima, 1981; Postma, 1982; Bahrig, 1985; Rajan et al., 1996). Siderite has also been identified in extraterrestrial materials such as meteorites (Johnson and Prinz, 1993; Romanek et al., 1994; Treiman and Romanek, 1998) and interplanetary dust particles (Keller et al., 1994). The geochemical and isotopic information stored in siderite provide valuable insights into the environmental conditions of mineral formation and the processes by which carbonate minerals are modified over time (Curtis et al., 1986; Curtis and Coleman, 1986; Mozley, 1989; Pye et al., 1990; Woods and Garrels, 1992; Ohmoto et al., 2004).

Siderite of biological origin is well documented. Prokaryotic microorganisms can reduce Fe(III) in surficial

* Corresponding authors. Present addresses: University of Kentucky, Department of Earth and Environmental Sciences, Lexington, KY 40506-0053, USA. Fax: +1 859 323 1938 (C.S. Romanek); Department of Microbiology, University of Granada, Campus Universitario de Cartuja, 18071 Granada, Spain (C. Jiménez-López).
E-mail addresses: c.romanek@uky.edu (C.S. Romanek), cjl@ugr.es (C. Jiménez-López).

0016-7037/$ - see front matter © 2009 Elsevier Ltd. All rights reserved.
doi:10.1016/j.gca.2009.05.065

environments and induce the precipitation of siderite under reducing conditions (Lovley and Phillips, 1988; Fredrickson et al., 1998). The reduction of Fe(III) is commonly coupled to the oxidation of organic compounds such as lactate and acetate, which can generate sufficient carbonate ion (CO_3^{2-}) to exceed the solubility limit for the solid (Roh et al., 2003). This process has been documented in the laboratory for a wide range of microorganisms (Roden and Lovley, 1993; Mortimer and Coleman, 1997; Mortimer et al., 1997; Zhang et al., 1998, 2001; Dong et al., 2000; Romanek et al., 2003). In these experiments, siderite is consistently formed under bicarbonate-buffered, Ca-free conditions resulting in the formation of fine grained rhombohedra (Mortimer and Coleman, 1997; Mortimer et al., 1997; Fredrickson et al., 1998; Roden et al., 2002). Microorganisms may also stimulate the formation of siderite by: (1) raising the pH of the environment through autotrophic processes that consume CO_2 (e.g., photosynthesis or CO_2 reduction), (2) releasing hydroxyl groups directly to the environment through dissimilatory metabolic processes such as the reduction of Fe- and Mn-(oxy)hydroxide minerals (Morse et al., 1992), or (3) through the ammonification of organic compounds (Castanier et al., 2000).

Siderite concretions are good examples of carbonate structures that are mediated by dissimilatory iron reducing bacteria (Curtis et al., 1986; Moore et al., 1992; Mozley and Carothers, 1992; Coleman and Raiswell, 1993; Duan et al., 1996). Many Fe-bearing carbonate cements found in rocks of the north slope of Alaska, the North Sea oil reservoirs and elsewhere are thought to have been influenced by microbial activity (Mozley and Carothers, 1992; Cortecci and Frizzo, 1993; Thyne and Gwinn, 1994). Some researchers have even hypothesized that siderite in Precambrian banded iron formations may be microbial in origin (Konhauser and Ferris, 1996).

Whereas the production of pure microbial siderite has been studied in detail, very little is known about microbially-mediated siderite that contains other cations (e.g., Ca and Mg) in its crystal structure (but see Roden et al., 2002). Notable among these are the works by Mortimer and Coleman (1997) and Mortimer et al. (1997) who measured the incorporation of Mg, Ca and Mn in siderite produced by dissimilatory iron reducing bacteria. Mortimer et al. (1997) demonstrated that Fe-reducing bacteria are capable of producing calcian and magnesian siderite at 25 °C from solutions containing solid Fe(III) oxyhydroxide, aqueous Ca (~3–8 mM) and aqueous Mg (~4–13 mM). In these experiments, they showed that the amount of Ca in the solid decreased as the metabolic activity of the bacteria increased. Assuming that metabolic activity and aqueous Fe(II) concentration are positively correlated in their experiments, the Ca content of their solids should be proportional to the Ca:Fe ratio of the solution from which they precipitated.

Our knowledge of the environmental factors that control the formation of inorganic siderite is based primarily on laboratory experiments. Most inorganic studies have synthesized siderite from metastable precursors under elevated temperatures or pressures (e.g., 33–197 °C and 100–500 bars: Carothers et al., 1988; 100 °C and 19 bars: Wersin et al., 1989 and Bruno et al., 1992) or from recrystallized precursors at temperatures from 35 to 70 °C (Johnson, 1990). Singer and Stumm (1970) were the first to precipitate inorganic siderite at a temperature below 30 °C under atmospheric pressure and a relatively low pCO_2 environment (<10% CO_2) analogous to most surficial environments. More recently, Jiménez-López and Romanek (2004) precipitated pure siderite using the methodology of Singer and Stumm (1970) while holding the physicochemical conditions of the precipitating fluid nearly constant throughout the crystallization process (i.e., chemo-stat type experiment) to study the precipitation kinetics and isotope systematics of siderite. They determined that pure siderite formed at rates almost five orders of magnitude lower than calcite under conditions of similar saturation state for each mineral. To date, no experiments have been undertaken to study the competing effect of other cations (Ca or Mg) on the formation of siderite at low temperature (e.g., 25 °C).

1.2. Siderite solid solutions in nature

The low temperature solid solution characteristics of siderite may be inferred from equilibrium assemblages of carbonate minerals grown at elevated pressure and temperature (Goldsmith and Heard, 1961; Goldsmith et al., 1962; Rosenberg, 1963a,b; Rosenberg, 1967; Anovitz and Essene, 1987) but the results contrast sharply with the chemical composition of natural siderites known to form below 100 °C (Fig. 1). Natural magnesite–siderite solid solutions show a significant incorporation of $CaCO_3$ (up to 20 mol%) in their structures that is clearly outside the

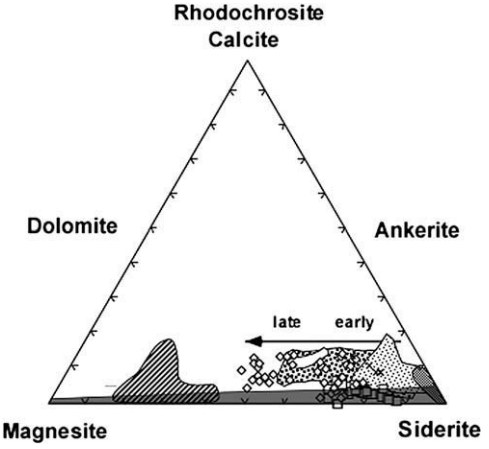

Fig. 1. Geochemistry of siderite (and magnesite) reported in the literature for deposits known to form at <100 °C. Apices denote the pure end-member carbonates for siderite ($FeCO_3$), magnesite ($MgCO_3$), and calcite + rhodochrosite ($CaCO_3 + MnCO_3$). References for symbols and fields: (1) hatched-line field: meteorites (Johnson and Prinz, 1993); (2) open diamonds: early to late burial of deep marine sediments (Mozley and Carothers, 1992); (3) open squares: siderite concretions (Curtis et al., 1986); (4) light and heavy stippled field: freshwater siderites of Ivishak formation (Mozley, 1989); (5) square-stippled field: freshwater siderites of Tyonek formation (Mozley, 1989); (6) X: tidal marsh siderites (Moore et al., 1992); (7) dark shadowed field: magnesite–siderite solid solution boundary for 250 °C (Anovitz and Essene, 1987).

range of equilibrium values predicted by Anovitz and Essene (1987) for higher temperatures (e.g., 250 °C). Interestingly, the theoretical trend predicted by Anovitz and Essene (1987) is for magnesite–siderite solid solutions to contain *less* $CaCO_3$ as the formation temperature decreases, which is opposite to observations based on the analysis of low temperature (<100 °C) deposits.

To better understand the factors that control the geochemistry of mixed cation carbonates at low temperature, a set of experiments was conducted where solid carbonate was precipitated inorganically from a range of solution compositions (Fe, Ca, Mg) at 25 and 70 °C. The lack of existing data on the precipitation kinetics and element partitioning behavior of mixed cation carbonates justified the use of free-drift experiments in this initial study. These experiments provide a starting point for future chemo-stat (constant chemistry) experiments that will more accurately elucidate the solid-solution relationships of mixed cation carbonates and provide a template upon which the origin of natural low temperature carbonates of similar chemistry may be reconciled.

2. MATERIALS AND METHODS

2.1. Materials

Sigma and Aldrich certified chemicals were used to prepare $NaHCO_3$, $Fe(ClO_4)_2$, $Ca(ClO_4)_2$ and $Mg(ClO_4)_2$ stock solutions in oxygen-free de-ionized water (Milli-Q). Oxygen free water was prepared by boiling de-ionized water in a container for 1 h. The container was then placed in a crushed ice bath and sparged with ultra-high purity N_2 that was previously passed over hot Cu metal until the fluid was cold. The container was then sealed and immediately placed inside an anaerobic chamber (Coy Laboratory Products Inc.; see below) where it was opened and allowed to degas further. Stock solutions (1.0 M) of $NaHCO_3$, $Fe(ClO_4)_2$, $Ca(ClO_4)_2$ and $Mg(ClO_4)_2$ were prepared separately inside the chamber, from which individual solutions of particular chemistry were made for each experimental run.

2.2. Methods

2.2.1. Experimental apparatus and analytical procedures

Experiments were performed at 25 °C and 1 atm total pressure inside the anaerobic chamber, which was filled with a H_2/N_2 (4% H_2) mixture. The chamber atmosphere was continually circulated through palladium catalyst fans to reduce trace O_2 to H_2O. The chamber also contained anhydrous $CaSO_4$ to trap any H_2O produced by the reaction of H_2 and O_2 on the catalyst. The chamber was equipped with gas analyzers to monitor $O_{2(g)}$, $H_{2(g)}$ and $CO_{2(g)}$ levels throughout the course of an experiment.

The pH of each solution was measured at the beginning and end of an experiment using an ORION pH meter. The pH electrode (Cole-Parmer) was calibrated with NIST-traceable standard buffer solutions for slope correction (pH 4 and 7) and temperature compensation. Based on periodic measurements of calibration standards, the accuracy for pH was estimated at ±0.05 (1σ SD).

The concentration of dissolved oxygen was screened using HACH AccuVac® Ampuls (indigo carime method) and a hand held spectrophotometer. All analyses were below the minimum detection limit of 6 μg/L O_2.

The total Fe, Ca and Mg concentration of the initial and final solutions was measured by inductively coupled plasma optical emission spectrometry (ICP-OES; Perkin-Elmer 4300DVS). A 1 mL sample of solution was acidified with oxygen-free HCl (0.5 M, 20 μL) to prevent the formation of a solid prior to analysis. Oxygen-free water was added to a final volume of 10 mL before the analysis. The analytical precision was better than 0.1 mM for each analyte based on the repeated measurement of certified aqueous standards (Inorganic Ventures, Inc.) that were diluted and matrix matched to solution compositions.

The alkalinity of the initial solution was determined from the volume and concentration of $NaHCO_3$ stock solution used to prepare the solution for each experimental run. The alkalinity of the final solution was determined based on the change in the sum of the aqueous divalent cation concentrations ($\Delta\Sigma_{cation}$) using the following equation: $\Delta\Sigma_{cation}/2 = \Delta_{alkalinity}$, which maintains the charge balance of the solution. The mass of solid produced over the course of each run was determined from $\Delta\Sigma_{cation}$ values and the 1:1 stoichiometry of cations to carbonate anion in an analogous manner.

The total Fe, Ca and Mg concentration of the solid was measured by ICP-OES. These analyses were performed by digesting 5 mg of solid in oxygen-free HCl (0.5 M, 1.0 mL) for 24 h at 70 °C and then diluting with oxygen-free water to a final volume of 10 mL. Analytical uncertainty for ICP-OES analysis was estimated at ±0.1 mM for Ca and ±0.2 mM for Fe and Mg, based on the repeated measurement of samples and standards (as above).

Solid mineralogy was determined using an X-ray diffractometer (Scintag, XGEN-4000). Powder samples were analyzed using Cu-*K*α radiation at an accelerating voltage of 45 kV and a filament current of 40 mA. Each sample was covered with a wax membrane during analysis to minimize surface oxidation. Instrumental offset in 2θ values was corrected using corundum (Al_2O_3) as an internal standard for each sample analysis. Mineralogical determinations were made based on the comparison of an observed diffractogram to those in the International Centre for Diffraction Data powder diffraction files (PDF).

Unit cell parameters for each experimental solid were calculated from the d-spacings (d) for a set of *hkl* reflections measured using the diffractometer. A multiple variable model of the following form was used: $z = a_1x + a_2y$, where $z = \frac{1}{d^2}$, $x = \frac{4(h^2+k^2+hk)}{3}$, and $y = l^2$. The unit cell parameters (a and c) were calculated using a least-square regression method which minimizes the difference $\sum[z_i - (a_1x_i + a_2y_i)]^2$ for the determination of the coefficients $a_1 = \frac{1}{a^2}$, and $a_2 = \frac{1}{c^2}$ for a particular set of *hkl* reflections. In this case, the methodology considered the six strongest reflections (Miller indices) for siderite (1 0 2, 1 0 4, 1 1 0, 1 1 3, 2 0 2, 1 1 6).

The morphology of crystals was characterized using a field emission scanning electron microscope (FE-SEM LEO 982). Samples were freeze-dried and gold-coated (150 Å thick) prior to SEM analysis.

The aqueous chemistry of the solution was evaluated using a modified version of the model described in Romanek et al. (1992) to determine the saturation state with respect to the pure end-member minerals siderite, calcite and magnesite. Saturation state was calculated by dividing the ionic activity product (IAP), defined as $a(x) \times aCO_3^{2-}$, where x = Fe, Ca or Mg, $a = m(x)\gamma(x)$, m(x) = molarity and $\gamma(x)$ = total activity coefficient, by the solubility product (K_{SP}) for the relevant pure mineral. Free activity coefficients were calculated for each dissociated species from measurements of pH, all cation and anion concentrations, and alkalinity using the Debye-Hückel equation. Total activity coefficients were determined by adjusting free activity coefficients to account for the percentage of a species that exists in the form of ion pairs or complexes. Perchlorate ion was considered as Cl^- because ion paring constants for $(ClO_4)^-$ are not available in the literature. This is a conservative assumption given that $(ClO_4)^-$ has a lower affinity to form complexes than Cl^-. All other association constants were estimated in a similar fashion or they were taken from Nordstrom et al. (1990). The solubility products for siderite and calcite were taken from Bruno et al. (1992) and Plummer and Busenberg (1982), respectively. Because of slow reaction kinetics, the solubility product for magnesite is poorly constrained, with published values that differ by over three orders of magnitude (Langmuir, 1973; Morse and Mackenzie, 1990). Hence, the value reported by Christ and Hostetler (1970) was arbitrarily chosen for this study. The temperature dependence for all association constants, equilibrium constants, and solubility products was considered when possible (Nordstrom et al., 1990; Romanek et al., 1992). Finally, because the ionic strength of the experimental solutions ranged between 0.10 and 0.34 (molar basis), the accuracy of the predicted saturation states are tentative. Nevertheless, the results provide a relative measure of the aqueous conditions and saturation states with respect to pure mineral phases. No attempt was made to calculate the solubility product for any solid solution given the composition of the solid probably changed throughout the course of each experiment. Moreover, significant errors may arise when performing these calculations due to the uncertainty in the solubility product for magnesite but this shortfall can only be corrected by more thorough solubility studies of the pure mineral and its solid solutions.

2.2.2. Experimental procedures

Twenty-one free-drift experiments were run over a 2–6 month period. Experimental solutions were prepared by mixing different aliquots of stock solution inside the anaerobic chamber to obtain solutions having the following range of concentrations: 25.0 and 60.0 mM for $NaHCO_3$, 0.0–61.2 mM for Fe(II), 0.0–26.1 mM for Ca and 0.0–57.5 mM for Mg (Table 1). The chemical composition of a solution was chosen to produce sufficient carbonate (g) for analysis within a meaningful time frame (months).

After an experimental solution was thoroughly mixed, the pH and dissolved O_2 content were measured and a 10 mL subsample was stored in an airtight vial (no head space) at 4 °C for further chemical analyses. The remaining solution was transferred to a 1 L bottle that was filled completely (no head space) and tightly closed with a flexible airtight lid. Eighteen bottles were stored in the anaerobic chamber at 25 °C, while three bottles were kept at 70 °C in a vacuum oven. At the conclusion of an experiment, each bottle was carefully opened so as to not disturb the solid that accumulated at the bottom of the vessel, and the pH and dissolved O_2 content of the solution were measured again. An aliquot of solution was then drawn from the top of the bottle into a syringe and filtered (0.2 μm syringe filter) into a 10 mL container for chemical analysis (as described above). The remaining solution was then thoroughly shaken and filtered (0.2 μm membrane) to collect the solid. The solid was rinsed twice with oxygen-free Milli-Q water (~5 s contact time) and stored under anaerobic conditions for further analysis.

3. RESULTS AND DISCUSSION

The results for the free-drift experiments are reported in Tables 1–3. Experimental runs FD-1 through FD-18 were conducted at 25 °C, whereas runs FD-19 through FD-21 were conducted at 70 °C. The initial pH of the experiments ranged from 6.3 to 7.8 depending on the initial solution chemistry, and the final pH ranged from 5.7 to 7.3. The final pH decreased significantly in each run because of the precipitation of solid carbonate which produced proton acidity. Only run FD-17 deviated from this trend where the pH decreased only 0.07 units over a 6-month period because little solid precipitated from solution.

The initial ionic strength of the solutions ranged from 0.10 to 0.34, whereas the final ionic strengths ranged from 0.05 to 0.24. Generally, the ionic strength of the solutions decreased over time because of the precipitation of a solid phase which removed ions from solution. The initial activity coefficients for the dissolved divalent cations ranged from 0.30 to 0.48 for Fe(II), 0.17 to 0.36 for Ca, and 0.21 to 0.40 for Mg (Table 2). Activity coefficients remained constant or they increased slightly (e.g., $\leq$0.05, except for runs FD-18, FD-19 and FD-20) throughout the course of each run. Saturation states at the beginning of each run were relatively high for siderite (1200–9200) compared to calcite (1.3–86) or magnesite (3.8–180). Saturation states decreased considerably over the course of each run due to the precipitation of a solid phase; for siderite, the values ranged from near equilibrium up to 90 (excluding run FD-15 at 370 and FD-20 at 280). A different outcome was observed for calcite and magnesite saturation states in the final solutions due to their higher relative solubilities. All of the final solutions were undersaturated with respect to calcite (except for runs FD-15 and FD-20) while the final solutions were undersaturated to supersaturated with respect to magnesite. Because most of the precipitates were not pure phases, but presumably heterogeneous solid solutions, the saturation state data provide only a crude assessment of the relative solubilities for the solids precipitated in this study. Despite the uncertainties in this analysis, the relatively low solubility for siderite has a profound effect on the chemistry of the final solutions and solids.

Table 1
Chemistry of the experimental solutions at the beginning and end of the free-drift experiments.

Run #	T (°C)	Time (mos)	$pH_{initial}$	pH_{final}	$NaHCO_3$ (mM) initial	$NaHCO_3$ (mM) final	Fe (II) (mM) initial	Fe (II) (mM) final	Ca (mM) initial	Ca (mM) final	Mg (mM) initial	Mg (mM) final	Ca/Fe initial	Mg/Fe initial
FD-1	25	3	6.31	5.70	25	14.1	25.0	3.1	0.0	0.0	0.0	0.0	0	0
FD-2	25	2	7.00	5.95	25	14.3	26.0	7.7	0.0	0.0	24.5	21.5	0	0.94
FD-3	25	3	6.88	5.89	25	6.4	24.9	0.3	26.1	15.3	26.4	24.7	1.05	1.06
FD-4	25	2	7.65	5.99	25	10.5	27.1	7.7	24.6	15.1	0.0	0.0	0.91	0
FD-5	25	3	6.96	5.75	25	9.8	27.6	0.7	5.1	2.5	28.8	27.9	0.18	1.05
FD-6	25	3	7.20	6.51	25	10.0	28.1	0.5	4.0	2.1	9.6	9.0	0.14	0.34
FD-7	25	3	7.20	6.32	25	10.8	27.9	1.6	2.5	0.5	9.6	9.4	0.09	0.34
FD-8	25	3	7.14	6.07	25	12.2	24.6	0.7	1.8	0.5	47.4	46.9	0.07	1.92
FD-9	25	3	7.19	6.35	25	9.4	29.3	0.6	1.6	0.4	43.4	42.2	0.05	1.48
FD-10	25	3	6.90	6.21	25	0.3	47.6	1.7	5.1	2.5	57.5	52.9	0.11	1.21
FD-11	25	3	7.10	5.92	25	Lost	61.2	Lost	4.9	Lost	11.1	Lost	0.08	0.18
FD-12	25	3	7.16	5.90	25	23.7	52.3	1.7	1.9	0.2	11.8	10.8	0.04	0.23
FD-13	25	3	6.95	5.78	25	0.3	55.2	1.7	1.4	0.5	50.4	46.0	0.03	0.91
FD-14	25	3	7.41	5.98	25	19.1	8.7	0.2	2.4	0.4	17.1	15.8	0.28	1.96
FD-15	25	2	7.73	7.12	60	54.7	2.0	0.5	2.1	0.8	52.9	45.2	1.02	26.02
FD-16	25	2	7.78	7.17	60	44.2	2.3	0.4	0.0	0.0	48.8	19.1	0	21.35
FD-17	25	6	7.35	7.28	60	60	0.0	0.0	0.0	0.0	56.1	56.1	–	–
FD-18	25	3	7.79	7.23	60	55.5	0.0	0.0	2.7	0.5	51.6	49.7	–	–
FD-19	70	2	7.76	7.21	60	35.6	0.0	0.0	0.0	0.0	53.9	5.1	–	–
FD-20	70	2	7.35	6.96	60	36.1	2.1	1.6	2.3	1.0	52.9	6.9	1.11	25.40
FD-21	70	2	7.56	7.03	60	37.3	1.9	0.1	0.0	0.0	53.1	9.6	0	27.84

Table 2
Results of Debye-Hückel model calculations of initial and final solution chemistry of the free-drift experiments.

Run #	Ionic strength[a]	γFe[b] (initial, final)	γCa (initial, final)	γMg (initial, final)	Ω[c] Siderite (initial, final)	Ω Calcite (initial, final)	Ω Magnesite (initial, final)
FD-1	0.10, 0.05	0.48, 0.50	–, –	–, –	7000, 50	–, –	–, –
FD-2	0.18, 0.13	0.38, 0.38	–, –	0.37, 0.40	2100, 30	–, –	9.2, 0.4
FD-3	0.25, 0.17	0.33, 0.34	0.30, 0.33	0.35, 0.38	1200, 10	11.8, 0.2	5.7, 0.2
FD-4	0.18, 0.11	0.38, 0.40	0.33, 0.38	–, –	9200, 30	85.7, 0.6	–, –
FD-5	0.19, 0.14	0.36, 0.36	0.33, 0.35	0.37, 0.40	1800, eq.	3.5, 0.1	8.2, 0.2
FD-6	0.14, 0.08	0.41, 0.42	0.36, 0.40	0.39, 0.44	3800, 10	5.7, 0.3	6.6, 0.6
FD-7	0.14, 0.08	0.42, 0.43	0.36, 0.41	0.40, 0.44	3900, 15	3.6, 0.1	6.7, 0.4
FD-8	0.26, 0.19	0.32, 0.33	0.30, 0.32	0.35, 0.37	2100, 5	1.7, 0.1	20, 0.9
FD-9	0.26, 0.18	0.32, 0.34	0.29, 0.33	0.34, 0.38	2400, 5	1.8, 0.1	20, 1.2
FD-10	0.34, 0.24	0.31, 0.31	0.28, 0.31	0.33, 0.37	2300, eq.	2.3, 0.1	11.2, 0.2
FD-11	0.25, l	0.37, l	0.33, l	0.37, l	6400, l	5.1, l	4.8, l
FD-12	0.21, 0.12	0.39, 0.39	0.34, 0.34	0.38, 0.38	6600, 20	2.5, 0.3	5.8, 5.9
FD-13	0.20, 0.22	0.31, 0.32	0.29, 0.32	0.34, 0.38	2700, eq.	1.3, 0.1	12.7, 0.2
FD-14	0.12, 0.08	0.40, 0.42	0.35, 0.38	0.39, 0.42	2300, 35	4.3, 0.8	20, 13.5
FD-15	0.22, 0.21	0.32, 0.32	0.24, 0.25	0.28, 0.29	1500, 370	12.5, 4.5	150, 130
FD-16	0.22, 0.14	0.32, 0.36	0.24, 0.29	0.28, 0.33	1800, 75	–, –	169, 16.2
FD-17	0.21, 0.23	–, –	–, –	0.29, 0.29	–, –	–, –	70, 70
FD-18	0.22, 0.16	–, –	0.24, 0.34	0.28, 0.39	–, –	14,.3 0.5	170, 20
FD-19	0.21, 0.11	–, –	–, –	0.21, 0.27	–, –	–, –	180, 20
FD-20	0.13, 0.12	0.30, 0.35	0.17, 0.27	0.30, 0.35	1400, 280	18.0, 3.4	3.8, 4.5
FD-21	0.22, 0.12	0.30, 0.35	–, –	0.23, 0.28	1400, 90	–, –	125, 25

l = sample lost prior to analysis.

[a] $I = 0.5\ \Sigma\ (m_i z_i^2)$, where I = ionic strength and m_i and z_i are the concentration and charge of ion "i".

[b] γ = total activity coefficient (as described in the text).

[c] Ω = saturation state (as defined in the text) for the pure mineral. The temperature dependence of K_{SP} for siderite and magnesite were not considered because these data are not available in the literature.

3.1. Experiments conducted at 25 °C

In run FD-1, aqueous Fe(II: ~25 mM) was the only divalent cation in solution, whereas in run FD-2 the solution contained similar concentrations of aqueous Fe(II) and Mg (~25 mM). Iron was the only cation detected in the wet chemical analysis of the solid carbonate from both experiments (Table 3). A different set of results occurred in run FD-3 which contained similar concentrations of aqueous Fe(II), Ca and Mg (~25 mM), and in run FD-4 which contained similar concentrations of aqueous Fe(II) and Ca (~25 mM). In these two experiments, Ca was detected in the Fe-carbonate at a concentration of 15 and 17 mol% $CaCO_3$, respectively, (see Table 3), while Mg was excluded from the solid in run FD-3 despite being present at a relatively high concentration in solution.

For runs FD-5 through FD-14, variable amounts of Ca were incorporated in the Fe-carbonate depending on the initial composition of the solution. In these runs, aqueous Fe(II) ranged from ~10 to 60 mM, Ca ranged from ~1.0 to 5.0 mM, and Mg ranged from ~10 to 60 mM. Despite the relatively wide range of solution chemistries, Mg was not observed in any of the solids while Ca was a ubiquitous constituent. In these runs, the Ca:Fe ratio of the solid [$Ca:Fe_{(s)}$] was correlated linearly to the Ca:Fe ratio of the initial solution [$Ca:Fe_{(aq)}$] according to the equation: $Ca:Fe_{(s)} = 0.268 \cdot [Ca:Fe_{(aq)}]$ ($r^2 = 0.741$; intercept fixed through the origin), while no statistically significant relationship was observed between $Ca:Fe_{(s)}$ and $Mg:Ca_{(aq)}$, or $Ca:Fe_{(s)}$ and $Mg:Fe_{(aq)}$. Furthermore, no statistically significant relationship was observed between $Ca:Fe_{(s)}$ and final solution composition.

Magnesium was detected in the Fe-carbonate precipitated in runs FD-15 and FD-16 when the aqueous HCO_3 concentration was increased to ~60 mM and aqueous Mg was increased to ~50 mM. In these two runs, the solid contained ~12–13 mol% $MgCO_3$ but differing amounts of $FeCO_3$ and $CaCO_3$ depending on the solution chemistry. In run FD-15, Fe(II) and Ca were minor constituents (~2.0 mM) of the solution yet they were significant components of the solid (59 mol% $FeCO_3$ and ~27 mol% $CaCO_3$), whereas in run FD-16, aqueous Ca was not a constituent of the solution and a magnesian siderite formed. These results suggest that the incorporation of Mg in the solid is independent of the Ca content of the solution or the solid in systems that produce $FeCO_3$ as the predominant crystalline phase.

In run FD-17, Mg was the only divalent cation in solution (~60 mM), and no precipitate formed even after a 6-month equilibration. Alternatively, in run FD-18, pure $CaCO_3$ precipitated from a solution containing aqueous Ca (~3 mM) and Mg (~50 mM).

3.2. Experiments conducted at 70 °C

Very different relationships were observed at 70 °C between the solutions and solids precipitated in runs FD-19 through FD-21. In these runs, the concentration of aqueous Mg was maintained at ~50 mM while aqueous Fe(II) and/or Ca was held at a concentration of ~2.0 mM. In run FD-19, a Mg-carbonate precipitated from a solution that contained Mg as the only divalent cation, whereas, in run FD-20, Fe(II) and Ca were included as constituents of the solution (~2 mM) and a mixed cation carbonate

Table 3
Solids precipitated from the free-drift experiments.

Run #	Time (mos)	T (°C)	Solid produced (g)	Fe (II: mM)	Ca (mM)	Mg (mM)	$X_{Fe(II),\ solid}$[b]	$X_{Ca,\ solid}$[b]	$X_{Mg,\ solid}$[b]	XRD
FD-1	3	25	2.8	56.21	–	–	100	0.0	0.0	Siderite
FD-2	2	25	2.6	41.78	–	0.00	100	0.0	0.0	Siderite
FD-3	3	25	4.5	23.17	4.22	0.00	84.6	15.4	0.0	Siderite[a]
FD-4	2	25	3.5	41.45	8.47	–	83.0	17.0	0.0	Siderite[a]
FD-5	3	25	3.8	30.01	1.75	0.00	94.5	5.5	0.0	Siderite[a]
FD-6	3	25	3.8	31.97	1.64	0.00	95.1	4.9	0.0	Siderite[a]
FD-7	3	25	3.6	31.29	0.84	0.00	97.4	2.6	0.0	Siderite[a]
FD-8	3	25	3.2	33.34	0.85	0.00	97.5	2.5	0.0	Siderite[a]
FD-9	3	25	3.9	34.12	0.84	0.00	97.6	2.4	0.0	Siderite[a]
FD-10	3	25	6.5	30.61	0.82	0.00	97.4	2.6	0.0	Siderite[a]
FD-11	3	25	–	33.58	0.85	0.00	97.5	2.5	0.0	Siderite[a]
FD-12	3	25	0.3	32.21	0.28	0.00	99.1	0.9	0.0	Siderite[a]
FD-13	3	25	7.3	33.91	0.32	0.00	99.1	0.9	0.0	Siderite[a]
FD-14	3	25	1.4	32.03	1.79	0.00	94.7	5.3	0.0	Siderite[a]
FD-15	2	25	1.0	12.91	5.97	2.90	59.3	27.4	13.3	Siderite[a]
FD-16	2	25	3.0	28.32	-	3.98	87.7	0.0	12.3	Siderite[a]
FD-17	6	25	–	–	–	–	–	–	–	No solid
FD-18	3	25	0.9	0.07	42.41	<0.01	0.0	100.0	0.0	Aragonite
FD-19	2	70	4.5	–	–	40.69	0.0	0.0	100.0	Hydromagnesite
FD-20	2	70	4.5	8.83	8.10	20.36	23.7	21.7	54.6	Magnesite[a]
FD-21	2	70	4.3	16.97	–	41.33	29.1	0.0	70.9	Magnesite[a]

[a] XRD pattern was shifted with respect to pure end-member.
[b] X is reported as percentage.

precipitated that contained ~22 mol% $CaCO_3$, ~24 mol% $FeCO_3$ and 55 mol% $MgCO_3$. Finally, in run FD-21 a solid containing ~29 mol% $FeCO_3$ and 71 mol% $MgCO_3$ precipitated from a solution containing aqueous Mg (~50 mM) and Fe(II: ~2 mM).

3.3. XRD analysis

3.3.1. Experiments conducted at 25 °C

Siderite was the only mineral identified in the XRD analysis of the solids precipitated in runs FD-1 through FD-16 (see Table 3). The diffractograms for runs FD-1 and FD-2 were diagnostic for siderite (PDF #29-0696), whereas the reflections for runs FD-3 through FD-16 deviated significantly because the crystal lattice was distorted from the pure Fe end-member due to the incorporation of Ca (and Mg) in the solid. In runs FD-3 through FD-14, Ca was the only cation (other than Fe) to be incorporated in siderite even though Mg was present in some solutions up to 60 mM. These solutions remained supersaturated/saturated with respect to siderite, while they all became undersaturated with respect to calcite (excluding run FD-15), and a few solutions remained saturated with respect to magnesite (i.e., runs FD-12, FD-14, FD-15 and FD-16) by the end of the runs.

Shifts in d-spacings (e.g., 1 0 2, 1 0 4, 1 1 0, 1 1 3, 2 0 2, 1 1 6) and the absence of peak splitting of the major reflections in the diffractograms clearly demonstrate that solid solutions of $FeCO_3$–$CaCO_3$, rather than separate phases (e.g., siderite and calcite), precipitated in runs FD-3 through FD-14. The effect of Ca on the crystal lattice is documented in Fig. 2 where the unit cell parameters (see Table 4) for the *a* (Fig. 2A) and *c* (Fig. 2B) axes are compared to the molar percentage of Ca in the bulk solid for runs FD-3 to FD-14. Most of the runs ($n = 10$) produced siderite containing less than 5 mol% $CaCO_3$ with *a* axis lengths that ranged between 4.6968 and 4.7198 Å, whereas runs FD-3 and FD-4 produced siderite that contained 15 and 17 mol% $CaCO_3$, respectively, with *a* axes that were significantly greater in length (4.7491 and 4.7379 Å). Considered collectively, these data are consistent with ideal mixing between the unit cell parameters of siderite and calcite. Interestingly, all the *a* axes were reduced in length by ~0.01 Å compared to the ideal mixing line of the pure end-members. A similar trend was observed for the estimated length of the *c* axis and molar percentage of Ca in the bulk solid (Fig. 2B), although in this case the empirical data more accurately reflected the ideal pure end-member mixing line.

Siderite was identified by XRD in runs FD-15 and FD-16 but these solids were distinct in chemical composition because they contained Fe and Mg ± Ca in the solid, having precipitated from solutions that contained relatively high aqueous Mg and HCO_3^- concentrations (50–60 mM). As such, the crystalline structures of these phases are discussed with runs FD-20 and FD-21 (see below).

3.3.2. Experiments conducted at 70 °C

In run FD-19, the hydrated magnesian carbonate hydromagnesite [$Mg_5(CO_3)_4(OH)_2{\cdot}4H_2O$] was identified by XRD analysis. This solid precipitated from a solution similar in chemistry to run FD-17 (which produced no solid at

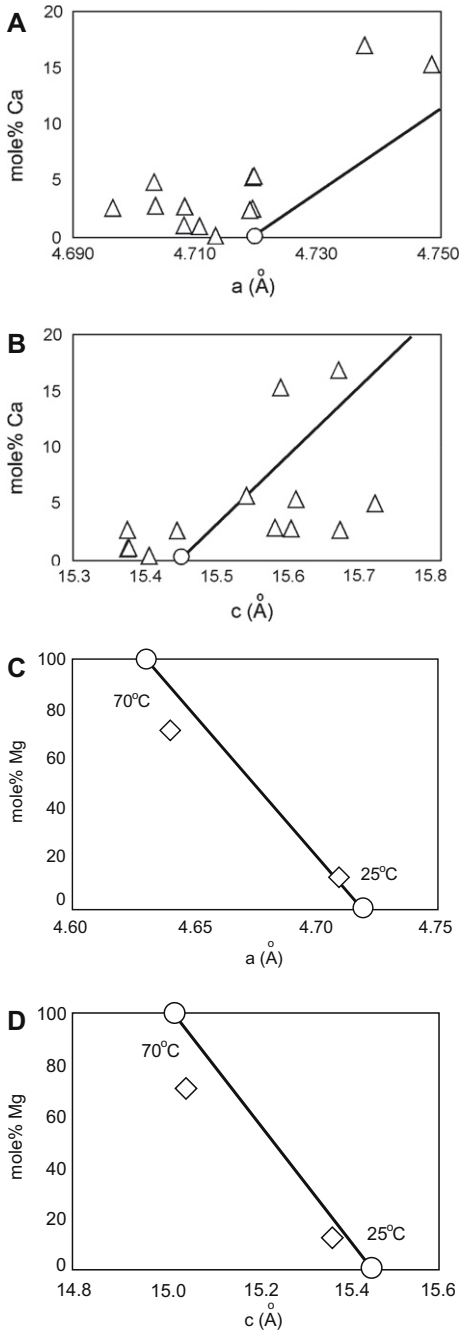

Fig. 2. Relationship between the percentage of Ca in the bulk solid and the unit cell parameters for the (A) *a* and (B) *c* crystallographic axes calculated from the Miller indices of the six most intense reflections (1 0 2, 1 0 4, 1 1 0, 1 1 3, 2 0 2, 1 1 6) identified in the X-ray diffractograms of experimental runs. Open triangles = experimental runs of this study; open circles = unit cell parameters for pure siderite (shown) and calcite (projected off the plot using solid line). Relationship between the percentage of Mg in the bulk solid and the unit cell parameters are plotted for runs FD-16 and FD-21 in (C) for the *a* and (D) *c* crystallographic axes as open diamonds. Open circles = unit cell parameters for magnesite (to the left) and siderite (to the right) connected by solid line.

Table 4
Results from unit cell parameter calculations for solids precipitated in this study.

Run #	*a* (A)	*c* (A)
FD-3	4.7491	15.5893
FD-4	4.7379	15.6709
FD-5	4.7198	15.5404
FD-6	4.7035	15.7203
FD-7	4.7037	15.5825
FD-8	4.7194	15.4447
FD-9	4.6968	15.6730
FD10	4.7085	15.6048
FD-11	4.7195	15.3764
FD-12	4.7084	15.3771
FD13	4.7108	15.3761
FD-14	4.7197	15.6109
FD-15	4.7668	15.6720
FD-16	4.7093	15.3673
FD-20	4.6924	15.3761
FD-21	4.6399	15.0464

25 °C). A Ca–Fe magnesite (22 mol% $CaCO_3$; 24 mol% $FeCO_3$) was identified by XRD in run FD-20 (solution chemistry equivalent to run FD-15), and a ferroan magnesite (29 mol% $MgCO_3$) was identified in run FD-21 (solution chemistry equivalent to run FD-16). In the latter two experiments, the solutions remained supersaturated with respect to magnesite and siderite (±calcite) throughout the run (see Table 2).

The relationships between the unit cell parameters and the extent of cation substitution for the siderite–magnesite solid solutions (runs FD-16 at 25 °C and FD-21 at 70 °C) are evaluated in Fig. 2C and D, respectively, for ease of presentation. As the percentage of $MgCO_3$ increases in the solid solution, the length of the *a* and *c* axes decrease, which is consistent with the trend in unit cell parameters for pure siderite and magnesite. These results suggest that a single phase solid solution of siderite–magnesite was produced in these runs and that the percentage of magnesite in the solid solution increased with temperature.

The relationships between the chemistry and unit cell parameters for the solids that contained Fe, Ca, and Mg in their crystal structure (i.e., runs FD-15 and FD-20) are more difficult to evaluate because three divalent cations participated in the precipitation reaction. The Microsoft Visual Basic™ software package IsoSource (version 1.3; Phillips and Gregg, 2003) was used to determine the *most likely* mixing ratio of magnesite, calcite and siderite that conformed with the unit cell parameters of each experimental solid (see Table 4). The program uses a simple three-component mass balance mixing model to quantify the distribution of all permissible sets of mixing ratios (within an arbitrarily defined tolerance) using the unit cell parameters for pure magnesite ($a = 4.63$; $c = 15.02$), siderite ($a = 4.72$; $c = 15.45$) and calcite ($a = 4.99$; $c = 17.06$), and the unit cell parameters (*a* and *c*) of each experimental solid. There were 37 possible solutions to the mass balance calculations for runs FD-15 and FD-20. For run FD-15, the closest possible match was a mixture of 55 mol% siderite, 25 mol% calcite, and 20 mol% magnesite, which is relatively close to the values obtained from the wet chemical analysis of the solid (59:27:13; see Table 3). For run FD-20, two preferred solutions emerged, a mixture of 30 (or 25) mol% siderite, 15 mol% calcite, and 55 (or 60) mol% magnesite. In this case, the theoretical mixtures were identical, within the error of the measurements, to the mixtures determined by the wet chemical analysis (23:22:55; see Table 3). Collectively, these observations suggest that the mixed cation (Fe–Ca–Mg) precipitates represent single phases that are accommodating all three cations structurally in the crystal lattice.

3.4. SEM analysis

The solid precipitated in runs FD-1 to FD-14 consisted of rhombohedra displaying characteristic (1 0 4) crystal faces with well-defined edges and vertices (Fig. 3). The edge length of pure to nearly pure siderite rhombohedra (e.g., runs FD-1, FD-2, and FD-13) ranged from 2 to 3 μm (Fig. 3A–C), with crystals increasing in size with the calcium content of the solid. For instance, the edge length for siderite crystals containing 2.5 and 5.5 mol% $CaCO_3$ (runs FD-11 and FD-5, respectively) ranged from 3 to 4 μm (Fig. 3D and E) whereas, for siderite containing 17.0 mol% $CaCO_3$ (run FD-4), it was 6–14 μm (Fig. 3F).

When Mg was incorporated in the crystal structure, the (1 0 4) crystal faces of siderite became considerably rougher (Fig. 4A and B). This texture is consistent with the roughening of crystal faces when Mg is incorporated in calcite (Busenberg and Plummer, 1989). Finally, the solid precipitated at 70 °C in runs FD-20 and FD-21 formed spherical aggregates about 6 μm in diameter that were composed of fine grained rhombohedra having smooth crystal faces and edge lengths of ~1 μm (Fig. 4C and D).

3.5. Dehydration as a potential controlling factor for mineral growth

In most solutions, divalent cations exist in the form of ion pairs (Fouillac and Criaud, 1984) and free ions that are bound to waters of hydration (Burgess, 1999). When these species sorb to carbonate surfaces or interact in the aqueous state, only a small percentage of molecules possess the energy required to fully dissociate and form a solid. This case holds true more so for aqueous Mg because of the relatively high dehydration energy for this ion compared to Ca or Fe(II). These dehydration energies are directly related to surface charge densities which increase from 0.1624 for Ca^{2+} to 0.2906 for Fe(II) to 0.3707 for Mg^{2+} (Lippmann, 1973). Thus, the energy required for Mg^{2+} to shed its inner and outer shells of hydration is relatively high compared to Fe^{2+} or Ca^{2+}. These relationships permit the growth and chemical evolution of carbonate minerals to be linked to the precipitation kinetics of the relevant solid phases (Lippmann, 1973; Burton and Walter, 1987; Brady et al., 1996; Arvidson and Mackenzie, 2000). Below, we interpret the chemical compositions of the carbonates formed in this study within this context.

Pure siderite precipitated in run FD-2 despite the fact that aqueous Mg was a major constituent (~25 mM) of

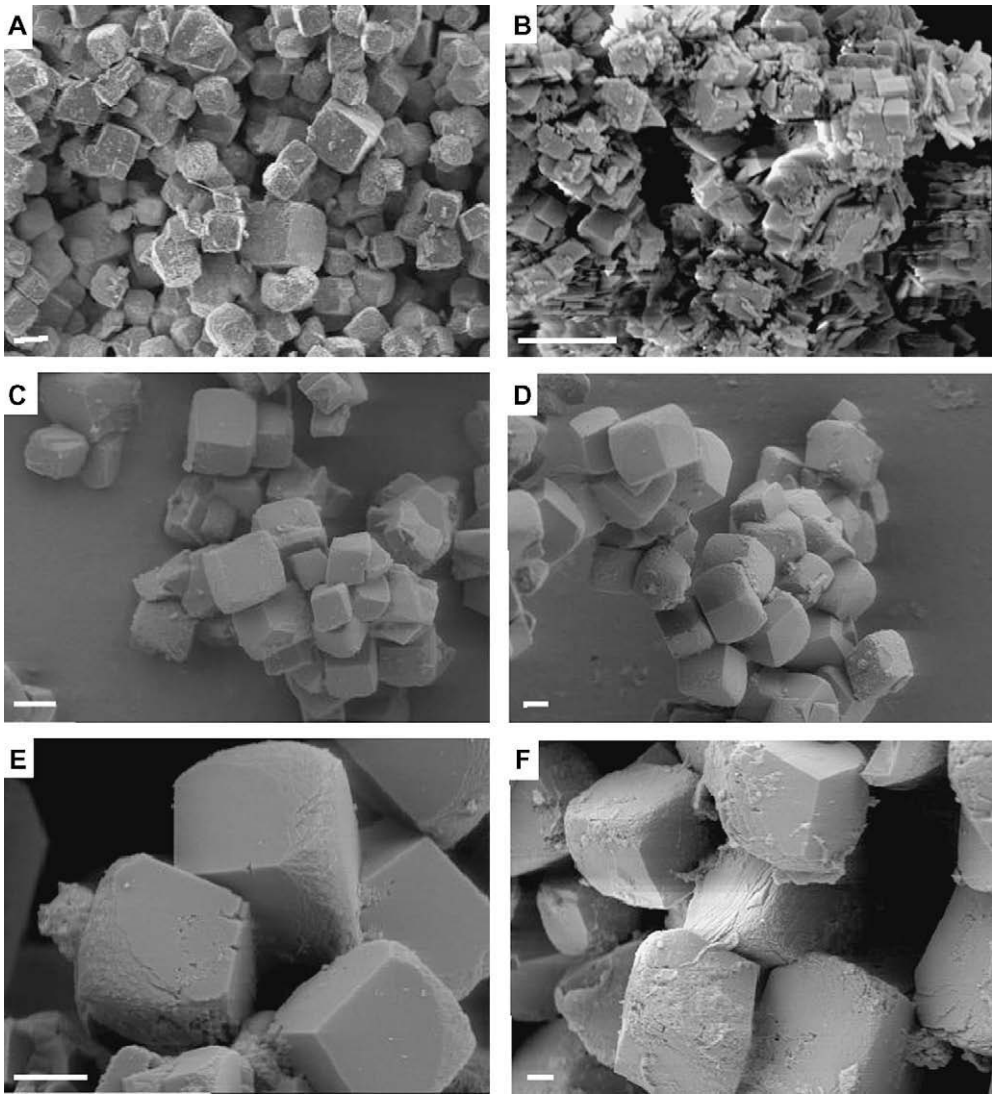

Fig. 3. SEM photomicrographs for solids precipitated in: (A) FD-1; (B) FD-2; (C) FD-13; (D) FD-11; (E) FD-5; (F) FD-4. All scale bars are 2 μm.

the parent solution. This result is consistent with the hypothesis that relative dehydration energies of aqueous Fe and Mg control the chemistry of the carbonate precipitate. In this case, there was insufficient energy in the aqueous system for Mg ions to shed their waters of hydration and be incorporated into siderite despite the initial parent solution being supersaturated with respect to magnesite. As siderite precipitation proceeded and the system approached chemical equilibrium, the dissolved carbonate became sufficiently depleted to preclude the formation of magnesite by the end of the experiment ($\Omega_{mag} \sim 0.4$). When Ca was introduced as an aqueous constituent (~25 mM) in runs FD-3 and FD-4, a calcian siderite precipitated (15–17 mol% $CaCO_3$). Even though Mg was included as an aqueous constituent in run FD-3 (~25 mM) it was not detected in the solid, suggesting that the presence of Ca (in the solution and solid Fe-carbonate) does not facilitate the incorporation of Mg in the crystal lattice.

The same set of processes explains the lack of Mg in the solid of runs FD-5 through FD-14, where Ca was incorporated in siderite over a range of aqueous Fe(II: ~10–60 mM) and Ca (up to 25 mM) concentrations even though aqueous Mg was present at up to ~60 mM. In three of these experiments (FD-9, FD-12, and FD-14) the solutions remained supersaturated with respect to magnesite throughout the duration of the experiment so the absence of magnesite cannot be attributed to its solubility under the experimental conditions. These results suggest that: (1) the factor(s) responsible for the exclusion of Mg from the crystal lattice do not inhibit the incorporation of Ca in siderite, and (2) the mechanism(s) controlling the incorporation of Mg in siderite are independent of the calcium content of the solid.

Unlike the previous experiments, Mg was incorporated in siderite in runs FD-15 and FD-16, when the aqueous HCO_3 and Mg concentrations were relatively high (60

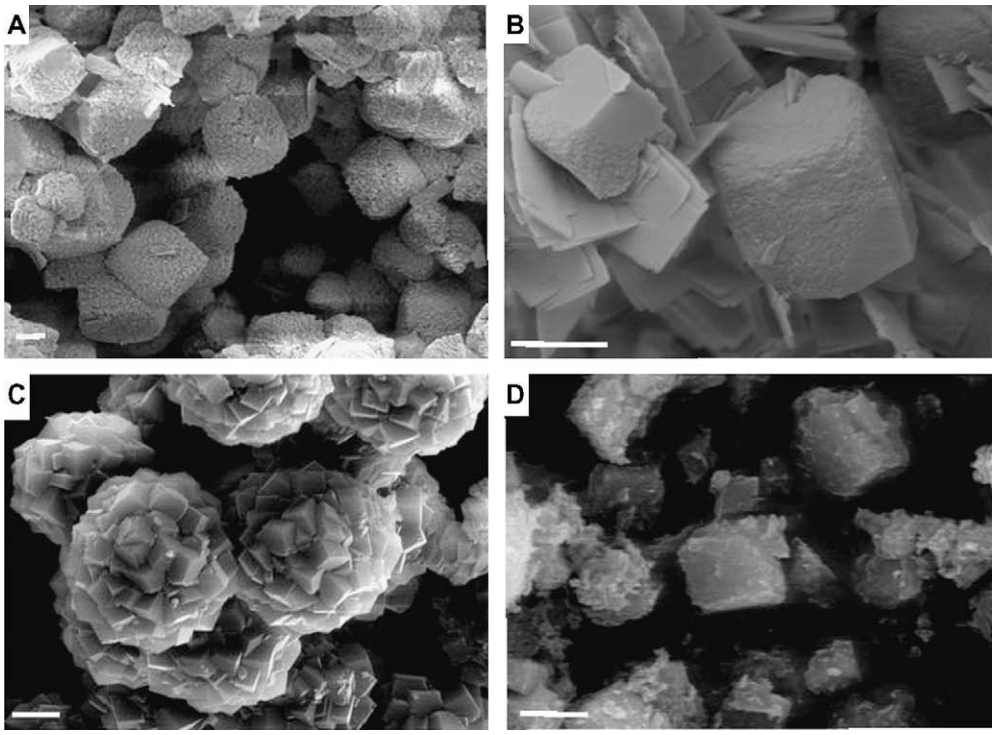

Fig. 4. SEM photomicrographs for solids precipitated in: (A) FD-15; (B) FD-16; (C) FD-20; (D) FD-21. All scale bars are 2 μm.

and ~50 mM, respectively) compared to Fe(II) and Ca (0 to ~2 mM). In these runs, the saturation state of the solution with respect to magnesite was approximately 10-fold greater than the earlier experiments while the saturation states with respect to siderite and calcite were similar. The significance of this finding is addressed below with the other experiments that produced an anhydrous Mg-carbonate solid.

Runs FD-17 and FD-18 did not contain aqueous Fe(II), nevertheless they provide additional insights into the incorporation of Mg in siderite by documenting the effect of Mg on the formation of $CaCO_3$ polymorphs. No solid precipitated in run FD-17 (Mg ~60 mM) whereas, in run FD-18, aragonite precipitated from a similar solution that contained a small amount of Ca (~3 mM). The formation of aragonite in run FD-18 is understandable given that the concentration of aqueous HCO_3 was raised to ~60 mM. It is well known that aqueous Mg inhibits the formation of calcite while it does not affect the precipitation kinetics of aragonite (Bischoff, 1968; Bischoff and Fyfe, 1968; Lippmann, 1973; Berner, 1975; Mucci and Morse, 1983; Deleuze and Brantley, 1997; Jiménez-López et al., 2004). Among other possibilities, aragonite may have precipitated at a faster rate than Mg could shed its waters of hydration for incorporation in calcite.

The lack of any solid in run FD-17 is harder to explain in light of the fact that Mg was incorporated (~13 mol% $MgCO_3$) in the calcian siderite produced in run FD-15. It appears that Mg dehydration may be facilitated by the presence of a pre-existing rhombohedral solid carbonate template. The crystal structure of the carbonate may provide a near-field environment that facilitates the dehydration of Mg at higher energy nucleation sites such as holes, kinks, or steps (Stephenson et al., 2008).

While the characterization of temperature effects was not a focal point of this investigation, three experiments (FD-19, FD-20, and FD-21) were conducted at 70 °C to better understand how temperature affects the crystal chemistry of the precipitates. In run FD-19, hydromagnesite precipitated from a solution that was supersaturated with respect to magnesite ($\Omega_{mag} \sim 180$), while the same run at 25 °C (FD-17: $\Omega_{mag} = 70$) failed to produce a precipitate. These results are consistent with a dehydration mechanism controlling the mineralogy of the precipitate as well. With the increase in temperature, the pH of solution in run FD-19 increased from 7.35 to 7.76 resulting in a fluid that exceeded saturation with respect to a phase (hydromagnesite) that did not require the dehydration of Mg prior to its incorporation in a solid. Likewise, Jiménez-López et al. (2004) identified hydromagnesite as the initial precipitate in free-drift experiments designed to grow Mg–calcite inorganically from solution at 25 °C. Although, the increase in temperature was sufficient to promote the growth of a hydrated Mg-carbonate, the added energy was insufficient to liberate aqueous Mg from its hydration sphere for the production of an anhydrous Mg-carbonate.

In run FD-20, a Ca–Fe magnesite (~22 mol% $CaCO_3$; ~24 mol% $FeCO_3$) formed from a solution that became slightly more supersaturated with respect to magnesite (Ω_{mag} evolved from 4 to 5) over the course of the experiment, while at 25 °C the same solution (FD-15: Ω_{mag} evolved from 150 to 130) produced a Mg–Ca siderite (~13 mol% $MgCO_3$; ~27 mol% $CaCO_3$). In these runs, the saturation state of the initial solution with respect to

siderite was relatively low ($\Omega_{sid} = 1500$ and 1400, respectively) compared to all of the other experiments and it remained relatively high ($\Omega_{sid} = 370$ and 280, respectively) at the end of the experiments, suggesting the incorporation of Mg in the solid slowed the precipitation kinetics of siderite considerably.

Runs FD-15 (at 25 °C) and FD-20 (at 70 °C) were the only experiments to produce a solid carbonate containing all three cations (Fe–Ca–Mg) in a single phase, with the proportion of Mg increasing and the proportion of Fe decreasing in the solid with temperature. The inverse correlation of Mg and Fe is consistent with the fact that these two divalent ions have charge densities and ionic radii that are more similar to each other than Ca. The incorporation of Mg in the solid of these two runs contrasts sharply with the lack of an anhydrous Mg-carbonate precipitate in runs FD-17, FD-18 or FD-19, which all contained aqueous Mg and HCO_3^- at relatively high concentration (~50 and 60 mM, respectively). As proposed earlier, this comparison reveals that a pre-existing *rhombohedral* solid carbonate surface may facilitate the dehydration of aqueous Mg for incorporation in the solid.

Finally, in run FD-21 a ferroan magnesite (~29 mol% $FeCO_3$) precipitated from a solution highly supersaturated with respect to magnesite ($\Omega_{mag} = 125$) at 70 °C, while the same solution (FD-16: $\Omega_{mag} = 170$) produced a magnesian siderite (12 mol% $MgCO_3$) at 25 °C. The incorporation of Mg in siderite at 25 °C and the formation of magnesite at 70 °C are consistent with a Mg dehydration mechanism that is both temperature dependent and surface facilitated.

4. PHASE EQUILIBRIA AND NATURAL CARBONATES

The chemistries of the carbonates precipitated in this study are compared to natural siderite–magnesite assemblages and synthetic phases of low temperature origin reported in the literature (Fig. 5). Most of the precipitates in this study fall within the boundary defined by natural siderite formed below 100 °C while fewer fall within the 250 °C field of siderite–magnesite solid solutions (Anovitz and Essene, 1987). Solids from runs FD-3 and FD-4, (>15 mol% CaCO3) and runs FD-15 and FD-20 (mixed Fe–Ca–Mg content) fall outside the range of values observed in nature. The absence of these phases in nature must be related to: (1) a lack of suitable aqueous environments that facilitate the formation of these compositions, (2) relative precipitation kinetics and mineral solubilities that preclude their formation, and/or (3) the production of reactive metastable phases that recrystallize over a relatively short time scale to produce calcite and siderite–magnesite solid solutions. The relatively large difference in charge density of Ca, compared to Fe and Mg undoubtedly contributes to the metastability of Ca-rich solid solutions. These observations may also explain the lack of the pure Fe end-member for dolomite [$CaFe(CO_3)_2$] at low temperature, which is predicted based on theoretical grounds (Reeder, 1983), but has yet to be found in nature.

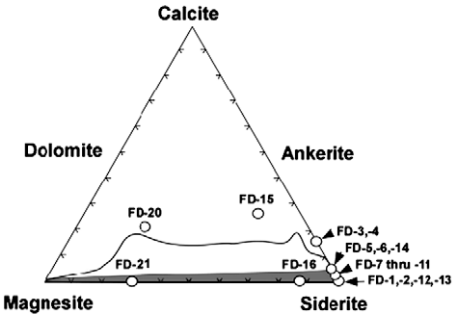

Fig. 5. Geochemistry of solid precipitates from this study superimposed on the ternary diagram of Fig. 1. Open circumscribed field contains all natural occurrences of siderite (Fig. 1) and natural magnesites reported in Möller (1989); shadowed field is siderite–magnesite solid solution boundary at 250 °C from Anovitz and Essene (1987).

4.1. Mixed cation carbonates as a potential fingerprint of organic–inorganic interactions

The formation of metastable mixed carbonates may be explained in part by system parameters (e.g., solution chemistry) and physicochemical processes (e.g., dehydration kinetics). Nevertheless, additional mechanistic details are required to account for the occurrence of the following naturally-occurring low temperature phases: (1) high Mg siderite formed microbially from aqueous solutions with low Mg concentrations (e.g., Mortimer et al., 1997), (2) microbial dolomite (e.g., Sánchez-Román et al., 2008a,b), and (3) bedded and lacustrine magnesite deposits (e.g., Möller, 1989; Thompson and Ferris, 1990).

Mirsal and Zankl (1985) proposed a mechanism by which a metal chelate facilitates the production of Mg-bearing carbonates at low temperature from solution. In their experiments, citric, tartaric, malonic and/or oxalic acids associated with specific transition metal ions (Me: Ni, Co, Fe(II), Mn, or Zn) are believed to form an octahedral transition metal ion chelate bound at various coordination positions by: (1) an organic-ligand (L), (2) a bicarbonate (HCO_3) or carbonate anion (CO_3), and (3) water molecules. For example, the Me-$(H)CO_3$-L chelate (where L = tridentate citrate) binds two hydrated $X(H)CO_{3(aq)}$ (where X = Ca, Mg) ion pairs at the carbonate site, initially as an outer-sphere complex (Fig. 6). Dehydration of at least one water molecule from the two $XCO_{3(aq)}$ ion pairs results in their detachment along with the inorganic carbonate anion from the Me-CO_3-L species, such that a $XCO_{3(aq)}$ dimer is released. Presumably, the XCO_3 dimer acts as the critical nucleus for further growth of Mg-bearing carbonate. In the overall reaction, the X-CO_3-L chelate promotes dehydration of the XCO_3 ion pair and, thus, dimerization.

Mirsal and Zankl (1985) showed that the potential for Ca uptake in solid carbonate increased from Ni → Co → Fe(II) → Mn → Zn as the central metal atom and that Mg uptake was enhanced in the opposite direction. These relationships may be rationalized on the basis of charge/radius ratio or electron density arguments, where Zn with the lower charge/radius ratio is more comparable to Ca, and Ni with the higher ratio, is more comparable to Mg. A similar

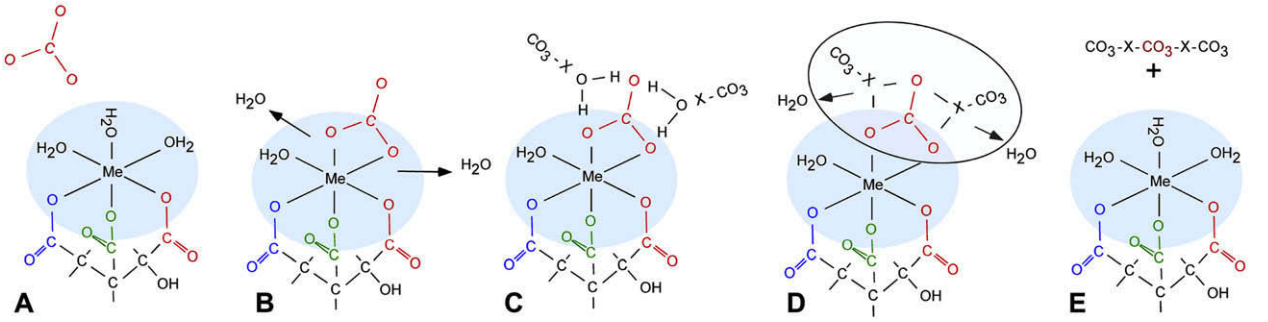

Fig. 6. Hypothetical mechanism for the generation of mixed cation carbonate minerals through organic-ligand promoted nucleation. (A) Hydrated metal chelate (in blue) composed of central metal atom (Me) bound with tridentate ligand (e.g., citrate); (B) carbonate anion displaces two water molecules at intermediate to basic pH; (C) hydrated metal (X) carbonate ion complex forms hydrogen bonds with carbonate; (D) ion complex sheds waters of hydration forming transition state (in circle); (E) carbonate dimer dissociates from chelate. Control of the cation chemistry of the dimer (X) is determined by the central metal atom in the chelate. Ni preferentially produces a $MgCO_3$ dimer while Zn produces a $CaCO_3$ dimer (modified from Mirsal and Zankl, 1985). (For interpretation of color mentioned in this figure legend the reader is referred to the web version of the article.)

mechanism may promote mixed cation carbonates, $XX'CO_3$ ($X \neq X'$), where XCO_3 and $X'CO_3$ ion-pairs attach to the Me-L chelate and eventually detach as a mixed dimer. In related work, polyaspartate peptide with a negative charge has been found to promote the incorporation of Mg into calcite (Stephenson et al., 2008), while the greater negative charge density associated with longer peptides is more efficient at promoting Ca ion dehydration kinetics (Elhadj et al., 2006). In the same context, molecular modeling studies have shown that the activation barrier for Ba^{2+} ion dehydration is lowered in the presence of sulfate and aspartate, which promotes attachment of Ba^{2+} to a $BaSO_4$ (barite) crystal surface (Piana et al., 2007; Jones et al., 2008).

Microbial metabolites, exudates or other cellular components (e.g., membranes, extra-polymeric substances) may function in the same capacity as Mirsal and Zankl's transition metal–organic chelates during the microbial reduction of Fe(III) to facilitate the formation of magnesian siderite or ferroan magnesite in natural environments at low temperature (25 °C). This hypothesis can only be tested through well designed experiments that are beyond the scope of this study, but if proven would produce a novel biosignature applicable equally to paleoenvironmental interpretations and planetary exploration.

4.2. Surface facilitated growth of mixed cation carbonates

Results from several of our experiments suggest that a pre-existing solid surface may catalyze the formation of preferred crystal chemistries. The solid surface may function in much the same way as the organic chelates of Mirsal and Zankl (1985) by providing surface-bound transition states that facilitate the dehydration of Mg. Lippmann (1973) states that the most stable configuration for the hydration sphere of a divalent cation is obtained when the dipole direction points to the center of the central cation, which maximizes the electrostatic energy of the ion-dipole bond, with deviation from this arrangement decreasing the energy of the bond. For the ions relevant to this study, the enthalpies of hydration increase from ~1300 to 2100 kJ/mole from CO_3^{2-} to Ca^{2+}, Fe^{2+} and finally Mg^{2+}. When hydrated ions adsorb onto the solid surface, they do not shed all their water molecules simultaneously, but through sequential stages of interaction on the crystal surface. Those water molecules that remain associated with an adsorbed cation become reoriented with the positive end of the dipole extending outward into the surrounding medium or linked by a hydrogen bond to a neighboring anion of the crystal surface (e.g., CO_3^{2-} group). Depending on the local bonding environment, the reorientation and interaction of water molecules with other ions undoubtedly lower the energy of the ion-dipole bond. Since the energy of interaction of one water molecule with a cation follows the same order as the enthalpies of hydration (~150 kJ/mol for Ca^{2+} to 190 kJ/mol for Fe^{2+} to 200 kJ/mol for Mg^{2+}; Table 21 in Lippmann, 1973), some configurations may lower the ion-dipole energy sufficiently for Mg to shed its hydration sphere and become incorporated in the solid.

Lippmann (1973) treats these interaction energies as barriers to precipitation and equates them to activation energies for the computation and comparison of relative reaction rates. His calculations suggest that the relative precipitation rates of magnesite and siderite are 10 and eight orders of magnitude lower, respectively, than calcite at similar saturation states. Whereas pure magnesite has yet to be precipitated from aqueous solutions in the laboratory at 25 °C, Jiménez-López and Romanek (2004) showed that the relative precipitation rate of inorganic siderite is approximately five orders of magnitude lower than that of calcite. These results are consistent with Lipmann's theoretical premise, at least for pure siderite, despite the considerable number of assumptions required in the analysis, and they provide some meaningful context for the factors that potentially control the formation of mixed cation carbonates.

It appears that extremely low precipitation rates preclude magnesite as a viable inorganic precipitate in low temperature environments. The only way to enhance the precipitation kinetics is to increase the concentration of Mg and CO_3^{2-} in solution but, as a result, the solubility

product for hydrated magnesian carbonate (e.g., hydromagnesite, see run FD-19) is exceeded first. Alternatively, the presence of an organic chelate may facilitate the production of this mineral in low temperature environments.

5. CONCLUSIONS

The inorganic synthesis of mixed cation (Fe–Ca–Mg) carbonates may be related to precipitation kinetics that are driven by the relative dehydration energies of the constituent cations that comprise the solid phase. Although Mg was a component of most of the experimental solutions of this study, it was excluded from the solid except at relatively high aqueous Mg and low Fe (±Ca) concentrations. Under these conditions, the presence of aqueous Ca did not facilitate the incorporation of Mg in the solid, nor was the percentage of Mg in the solid dependent on the Ca content of the solid. Alternatively, Mg was the primary component of all the solids precipitated at 70 °C. Considered collectively, these results suggest that the incorporation of Mg in anhydrous carbonates involves the dehydration of Mg on a pre-existing surface as the rate limiting step.

ACKNOWLEDGEMENTS

CJL acknowledges support from grants CGL2004-03910 and CGL2007-63859 from MEC (Spain) and the Fulbright/MEC Program. NS acknowledges funding support from NSF EAR CAREER 0208036 and ACS PRF 47792-AC2. The contribution of MC was carried out at the Jet Propulsion Laboratory (JPL), California Institute of Technology, under contract with the National Aeronautics and Space Administration (NASA), partly supported by JPL's Research and Technology Development Program (grant 01STCR-R.07.023.011). This work was also supported in part by NASA's Astrobiology Institute, NASA's Ancient Martian Meteorite program, and the US Department of Energy through Financial Assistance Award No. DE-FC09-96-SR18546 to the University of Georgia Research Foundation. Lindy Paddock, Brian Jackson, John Shields and the Junta de Andalucia research group BIO-103 are acknowledged for analytical assistance. Finally, J. Morse and A. Mucci are thanked for reviewing previous versions of this manuscript.

REFERENCES

Anovitz L. M. and Essene E. J. (1987) Phase-equilibria in the system $CaCO_3$–$MgCO_3$–$FeCO_3$. *J. Petrol.* **28**, 389–414.

Arvidson R. S. and Mackenzie F. T. (2000) Temperature dependence of mineral precipitation rates along the $CaCO_3$–$MgCO_3$ join. *Aquatic Chem.* **6**, 249–256.

Bahrig B. (1985) Paleo-environment information from deep water siderite (Lake of Laach, West Germany). In *Lacustrine Petroleum Source Rocks*, vol. 40 (eds. A. J. Fleet, K. Kelts and M. R. Talbot). Geol. Soc. Spec. Publ., pp. 153–158.

Berner R. A. (1975) The role of magnesium in the crystal growth of calcite and aragonite from sea water. *Geochim. Cosmochim. Acta* **39**, 489–504.

Bischoff J. L. (1968) Kinetics of calcite nucleation. Magnesium inhibition and ionic strength catalysis. *J. Geophys. Res.* **73**, 3315–3322.

Bischoff J. L. and Fyfe W. S. (1968) The aragonite–calcite transformation. *Amer. J. Sci.* **266**, 65–79.

Brady P. V., Krumhansl J. L. and Papenguth H. W. (1996) Surface complexation clues to dolomite growth. *Geochim. Cosmochim. Acta* **60**, 727–731.

Bricker O. P. (1975) Environmental factors in the inorganic chemistry of natural systems: the estuarine sediment environment. In: *Environmental Inorganic Chemistry* (ed. K. J. Irgolic). pp. 135–153.

Bruno J., Wersin P. and Stumm W. (1992) On the influence of carbonate in mineral dissolution: II. The solubility of FeCO3(s) at 25 °C and 1 atm total pressure. *Geochim. Cosmochim. Acta* **56**, 1149–1155.

Burgess J. (1999) *Ions in Solution: Basic Principles of Chemical Interactions*. Howood Publishing, Chichester England, 222.

Burton E. A. and Walter L. M. (1987) Relative precipitation rates of aragonite and Mg calcite from seawater–temperature or carbonate ion control. *Geology* **15**, 11–114.

Busenberg E. and Plummer L. N. (1989) Thermodynamics of magnesian calcite solid-solutions at 25 °C and 1 atm total pressure. *Geochim. Cosmochim. Acta* **53**, 1189–1208.

Carothers W. W., Adami L. H. and Rosenbauer R. J. (1988) Experimental oxygen isotope fractionation between siderite–water and phosphoric acid liberated CO_2–siderite. *Geochim. Cosmochim. Acta* **52**, 2445–2450.

Castanier S., Le Métayer-Levrel G., Orial G., Loubière J. F. and Pethuisot J. P. (2000) Bacterial carbonatogenesis and applications to preservation and restoration of historic property. In *Of Microbes and Art: the Role of Microbial Communities in the Degradation and Protection of Cultural Heritage* (eds. O. Ciferri, P. Tiano and G. Mastromei). Plenum, New York, pp. 203–218.

Christ C. L. and Hostetler P. B. (1970) Studies in the system MgO–SiO_2–CO_2–H_2O (II): the activity-product constant of magnesite. *Am. J. Sci.* **268**, 439–453.

Coleman M. L. and Raiswell R. (1993) Microbial mineralization of organic matter: mechanisms of self-organization and inferred rates of precipitation of diagenetic minerals. *Phil. Trans. R. Soc. Lond. A* **344**, 69–87.

Cortecci G. and Frizzo P. (1993) Origin of siderite deposits from the Lombardy Valleys, Northern Italy – a carbon, oxygen and strontium isotope study. *Chem. Geol.* **105**, 293–303.

Curtis C. D. and Coleman M. L. (1986) Controls on the precipitation of early diagenetic calcite, dolomite and siderite concretions in complex depositional sequences. In *Roles of Organic Matter in Sediment Diagenesis*, vol. 38 (ed. D. L. Gautier). Soc. Econ. Paleontol. Mineral. Spec. Pub., pp. 23–33.

Curtis C. D., Coleman M. L. and Love L. G. (1986) Pore water evolution during sediment burial from isotopic and mineral chemistry of calcite, dolomite and siderite concretions. *Geochim. Cosmochim. Acta* **50**, 2321–2334.

Deleuze M. and Brantley S. (1997) Inhibition of calcite crystal growth by Mg^{2+} at 100 °C and 100 bars: influence of growth regime. *Geochim. Cosmochim. Acta* **7**, 1475–1485.

Dong H. L., Fredrickson J. K., Kennedy D. W., Zachara J. M., Kukkadapu R. K. and Onstott T. C. (2000) Mineral transformation associated with the microbial reduction of magnetite. *Chem. Geol.* **169**, 299–318.

Duan W. M., Hedrick D. B., Pye K., Coleman M. L. and White D. C. (1996) A preliminary study of the geochemical and microbiological characteristics of modern sedimentary concretions. *Limnol. Oceanogr.* **41**, 1404–1414.

Elhadj S., Salter E. A., Wierzbicki A., DeYoreo J. J., Han N. and Dove P. M. (2006) Peptide controls on calcite mineralization: polyaspartate chain length affects growth kinetics and acts as a stereochemical switch on morphology. *Cryst. Growth Des.* **6**, 197–201.

Emerson S. (1976) Early diagenesis in anaerobic lake sediments: chemical equilibria in interstitial waters. *Geochim. Cosmochim. Acta* **40**, 925–934.

Fisher Q. J., Raiswell R. and Marshall J. D. (1998) Siderite concretions from nonmarine shales (Westphalian A) of the Pennines England: controls of their growth and composition. *J. Sediment. Res.* **68**, 1034–1045.

Fouillac C. and Criaud A. (1984) Carbonate and bicarbonate trace-metal complexes – critical reevaluation of stability-constants. *Geochem. J.* **18**, 297–303.

Fredrickson J. K., Zachara J. M., Kennedy D. W., Dong H., Onstott T. C., Hinman N. W. and Li S. M. (1998) Biogenic iron mineralization accompanying the dissimilatory reduction of hydrous ferric oxide by a groundwater bacterium. *Geochim. Cosmochim. Acta* **62**, 3239–3257.

Garrels R. M., Perry E. A. and Mackenzie F. T. (1973) Genesis of Precambrian iron-formations and development of atmospheric oxygen. *Econ. Geol.* **68**, 1173–1179.

Goldsmith J. R. and Heard H. C. (1961) Subsolidus phase relations in the system $CaCO_3$–$MgCO_3$. *J. Geol.* **69**, 45–74.

Goldsmith J. R., Graf D. L., Witters J. and Northrop D. A. (1962) Studies in the system $CaCO_3$–$MgCO_3$–$FeCO_3$. 1. Phase relations. 2. A method for major-element spectrochemical analysis. 3. Compositions of some ferroan dolomites. *J. Geol.* **70**, 659–688.

Hangari K. M., Ahmad S. N. and Perry E. C. (1980) Carbon and oxygen isotope ratios in diagenic siderite and magnetite from Upper Devonian Ironstone, Wadi Shatti District. *Libya. Econ. Geol.* **75**, 538–545.

James H. L. (1966) Chemistry of the Iron-rich Sedimentary Rocks. US Geol. Surv. Prof.l Pap. 440-W. p. 61.

Jiménez-López C., Romanek C. S., Huertas F. J., Ohmoto H. and Caballero E. (2004) Oxygen isotope fractionation in synthetic magnesian calcite. *Geochim. Cosmochim. Acta* **68**, 3367–3377.

Jiménez-López C. and Romanek C. S. (2004) Precipitation kinetics and carbon isotope partitioning of inorganic siderite at 25 °C and 1 atm. *Geochim. Cosmochim. Acta* **68**, 557–571.

Johnson M. L. (1990) Ferrous Carbonate Precipitation Kinetics. A Temperature Ramped Approach. Ph. D. Rice University, Houston TX.

Johnson C. A. and Prinz M. (1993) Carbonate compositions in CM and CI chondrites, and implications for aqueous alteration. *Geochim. Cosmochim. Acta* **57**, 2843–2852.

Jones F., Piana S. and Gale J. D. (2008) Understanding the kinetics of barium sulfate precipitation from water and water–methanol solutions. *Cryst. Growth Des.* **8**, 817–822.

Keller L. P., Thomas K. L. and McKay D. S. (1994) The nature of carbon-bearing phases in hydrated interplanetary dust particles. *Meteoritics* **29**, 480–481.

Konhauser K. O. and Ferris F. G. (1996) Diversity of iron and silica precipitation by microbial mats hydrothermal waters, Iceland: implications for Precambrian iron formations. *Geology* **24**, 323–326.

Langmuir D. (1973) Stability of carbonates in the system MgO–CO_2–H_2O. *J. Geol.* **73**, 730–745.

Lippmann F. (1973) *Sedimentary Carbonate Minerals*. Springer-Verlag, Berlin, 228.

Lovley D. R. and Phillips E. J. P. (1988) Novel mode of microbial energy metabolism: organic carbon oxidation coupled to dissimilatory reduction of iron or manganese. *Appl. Environ. Microbiol.* **54**, 1472–1480.

Matsumoto R. and Iijima A. (1981) Origin and diagenetic evolution of Ca–Mg–Fe carbonates in some coalfields of Japan. *Sedimentology* **28**, 239–259.

Maynard J. B. (1982) Extension of Berner's "new geochemical classification of sedimentary environments" to ancient sediments. *J. Sediment. Petrol.* **52**, 1325–1331.

Mirsal I. A. and Zankl H. (1985) Some phenomenological aspects of carbonate geochemistry – the control effect of transition-metals. *Geol. Rundsch.* **74**, 367–377.

Möller P. (1989) Minor and trace elements in magnesite. In: *Magnesite Geology, Mineralogy, Geochemistry, Formation of Mg-Carbonates*, (ed. P. Möller), Monograph Series on Mineral Deposits 28. Gebrüder Borntraeger, Berlin. pp. 173–195.

Morse J. W. and Mackenzie F. T. (1990) *Geochemistry of Sedimentary Carbonates, Developments in Sedimentology, vol. 48*. Elsevier, Amsterdam, 707.

Moore S. E., Ferrell J. R. E. and Aharon P. (1992) Diagenetic siderite and other ferroan carbonates in a modern subsiding marsh sequence. *J. Sediment. Petrol.* **62**, 357–366.

Morse J. W., Cornwell J. C., Arakaki T., Lin S. and Huerta-Diaz M. (1992) Iron sulfide and carbonate mineral diagenesis in Baffin-Bay Texas. *J. Sediment. Petrol.* **62**, 671–680.

Mortimer R. J. G. and Coleman M. L. (1997) Microbial influence on the oxygen isotopic composition of diagenetic siderite. *Geochim. Cosmochim. Acta* **61**, 1705–1711.

Mortimer R. J. G., Coleman M. L. and Rae J. E. (1997) Effect of bacteria on the elemental composition of early diagenetic siderite: implications for palaeoenvironmental interpretations. *Sedimentology* **44**, 759–765.

Mozley P. S. (1989) Relationship between depositional environments and the elemental composition of early diagenetic siderite. *Geology* **17**, 704–706.

Mozley P. S. and Carothers W. W. (1992) Elemental and isotopic composition of siderite in the Kupanuk formation, Alaska: effect of microbial activity and water/sediment interaction on early pore-water chemistry. *J. Sediment. Petrol.* **64**, 681–692.

Mucci A. and Morse J. W. (1983) The incorporation of $Mg^{2+}$and Sr^{2+}into calcite overgrowths: influences of growth rate and solution composition. *Geochim. Cosmochim. Acta* **47**, 217–233.

Nordstrom D. K., Plummer L. N., Langmuir D., Busenberg E., May H. M., Jones B. F. and Parkhurst D. L. (1990) Revised chemical equilibrium data for major water–mineral reactions and their limitations. In *Chemical Modeling of Aqueous Systems II* (eds. D. C. Bassett and R. L. Melchior). American Chemical Society, Washington, DC, pp. 398–413.

Ohmoto H., Watanabe Y. and Kumazawa K. (2004) Evidence from massive siderite beds for a CO_2-rich atmosphere before 1.8 billion years ago. *Nature* **29**, 395–399.

Phillips D. L. and Gregg J. W. (2003) Source partitioning using stable isotopes: coping with too many sources. *Oecologia* **136**, 261–269.

Piana S., Jones F. and Gale J. D. (2007) Aspartic acid as a crystal growth catalyst. *CrystEngComm* **9**, 1187–1191.

Plummer L. N. and Busenberg E. (1982) The solubilities of calcite, aragonite and vaterite in CO_2–H_2O solutions between 0 and 90 °C and an evaluation of the aqueous model for the system $CaCO_3$–CO_2–H_2O. *Geochim. Cosmochim. Acta* **46**, 1011–1040.

Postma D. (1982) Pyrite and siderite formation in brackish and fresh-water swamp sediments. *Am. J. Sci.* **282**, 1151–1183.

Pye K., Dickson A. D., Schiavon N., Coleman M. L. and Cox M. (1990) Formation of siderite–Mg-calcite–iron sulphide concretions in interstidal marsh and sandflat sediments, north Norfolk, England. *Sedimentology* **37**, 325–343.

Rajan S., Mackenzie F. T. and Glenn C. R. (1996) A thermodynamic model for water column precipitation of siderite in the Plio-Pleistocene Black Sea. *Am. J. Sci.* **296**, 506–548.

Reeder R. J. (1983) Crystal chemistry of the rhombohedral carbonates. In *Carbonates: Mineralogy and Chemistry, Reviews in Mineralogy*, vol. 11 (ed. R. Reeder). Bookcrafters, Chelsea, MI, pp. 1–47.

Roden E. E. and Lovley D. R. (1993) Dissimilatory Fe(III) reduction by the marine microorganism desulfuromonas–acetoxidans. *Appl. Environ. l Microbiol.* **59**, 734–742.

Roden E. E., Leonardo M. R. and Ferris F. G. (2002) Immobilization of strontium during iron biomineralization coupled to dissimilatory hydrous ferric oxide reduction. *Geochim. Cosmochim. Acta* **66**, 2823–2839.

Roh Y., Zhang C. L., Vali H., Lauf R. J., Zhou J. and Phelps T. J. (2003) Biogeochemical and environmental factors on iron biomineralization: magnetite and siderite formation. *Clays Clay Min.* **51**, 83–95.

Romanek C. S., Grady M. M., Wright I. P., Mittlefehldt D. W., Socki R. A., Pillinger C. T. and Gibson, Jr., E. K. (1994) Record of fluid-rock interactions on Mars from the meteorite ALH84001. *Nature* **372**, 655–657.

Romanek C. S., Grossman E. L. and Morse J. W. (1992) Carbon isotopic fractionation in synthetic aragonite and calcite: effects of temperature and precipitation rate. *Geochim. Cosmochim. Acta* **56**, 419–430.

Romanek C. S., Zhang C. L., Li Y. L., Horita J., Vali H., Cole D. R. and Phelps T. J. (2003) Carbon and hydrogen isotope fractionations associated with dissimilatory iron-reducing bacteria. *Chem. Geol.* **195**, 5–16.

Rosenberg P. E. (1963a) Synthetic solid solutions in systems $MgCO_3$–$FeCO_3$ and $MnCO_3$–$FeCO_3$. *Am. Mineral.* **48**, 1396–1400.

Rosenberg P. E. (1963b) Subsolidus relations in system $CaCO_3$–$FeCO_3$. *Am. J. Sci.* **261**, 683–690.

Rosenberg P. E. (1967) Subsolidus relations in system $CaCO_3$–$MgCO_3$–$FeCO_3$ between 350 and 550 °C. *Am. Mineral.* **52**, 787–796.

Sánchez-Román M., Vasconcelos C., Warthmann R., Rivadeneyra M. A., McKenzie J. A., (2008a) Microbial Dolomite Precipitation under Aerobic Conditions: Results from Brejo do Espinho Lagoon (Brazil) and Culture Experiments. IAS Spec. Publ., vol. 40. pp. 167–178.

Sánchez-Román M., Vasconcelos C., Schmid T., Dittrich M., McKenzie J. A., Zenobi R. and Rivadeneyra M. A. (2008b) Aerobic microbial dolomite at the nanometer scale: implications for the geologic record. *Geology* **36**, 879–882.

Singer P. C. and Stumm W. (1970) The solubility of ferrous iron in carbonate-bearing waters. *J. Am. Water Works Assoc.* **62**, 198–202.

Stephenson A. E., DeYoreo J. J., Wu L., Wu K. J., Hoyer J. and Dove P. M. (2008) Peptides enhance magnesium signature in calcite: insights into origins of vital effects. *Science* **322**, 724–727.

Thompson J. B. and Ferris F. G. (1990) Cyanobacterial precipitation of gypsum, calcite, and magnesite from natural alkaline lake water. *Geology* **18**, 995–998.

Thyne G. D. and Gwinn C. J. (1994) Evidence for a paleoaquifer from early diagenetic siderite of the cardium formation, Alberta. *Canada J. Sediment. Res.* **64**, 726–732.

Treiman A. H. and Romanek C. S. (1998) Bulk and stable isotopic composition of carbonate minerals in Martian meteorite Allan Hills 84001: no proof of high formation temperature. *Meteor. Planet. Sci.* **33**, 737–742.

Wersin P., Charlet L., Karthein R. and Stumm W. (1989) From adsorption to precipitation: sorption of Mn^{2+} on $FeCO_{3(s)}$. *Geochim. Cosmochim. Acta* **53**, 2787–2796.

Woods T. L. and Garrels R. M. (1992) Calculated aqueous-solution–solid-solution relations in the low temperature systems CaO–MgO–FeO–CO_2–H_2O. *Geochim. Cosmochim. Acta* **56**, 3031–3143.

Zhang C. L., Vali H., Romanek C. S., Roh Y., Sears S. K. and Phelps T. J. (1998) Chemical and morphological characterization of siderite formed by iron reducing bacteria. *Am. Mineral.* **61**, 927–932.

Zhang C. L., Horita J., Cole D. R., Zhou J., Lovley D. R. and Phelps T. J. (2001) Temperature-dependent oxygen and carbon isotope fractionation of biogenic siderite. *Geochim. Cosmochim. Acta* **65**, 2257–2271.

Associate editor: Alfonso Mucci